

Study of the electromagnetic Dalitz decay $J/\psi \rightarrow e^+e^-\pi^0$

M. Ablikim¹, M. N. Achasov^{4,c}, P. Adlarson⁷⁶, O. Afedulidis³, X. C. Ai⁸¹, R. Aliberti³⁵, A. Amoroso^{75A,75C}, Q. An^{72,58,a}, Y. Bai⁵⁷, O. Bakina³⁶, I. Balossino^{29A}, Y. Ban^{46,h}, H.-R. Bao⁶⁴, V. Batzskaya^{1,44}, K. Begzsuren³², N. Berger³⁵, M. Berlowski⁴⁴, M. Bertani^{28A}, D. Bettoni^{29A}, F. Bianchi^{75A,75C}, E. Bianco^{75A,75C}, A. Bortone^{75A,75C}, I. Boyko³⁶, R. A. Briere⁵, A. Brueggemann⁶⁹, H. Cai⁷⁷, X. Cai^{1,58}, A. Calcaterra^{28A}, G. F. Cao^{1,64}, N. Cao^{1,64}, S. A. Cetin^{62A}, J. F. Chang^{1,58}, G. R. Che⁴³, G. Chelkov^{36,b}, C. Chen⁴³, C. H. Chen⁹, Chao Chen⁵⁵, G. Chen¹, H. S. Chen^{1,64}, H. Y. Chen²⁰, M. L. Chen^{1,58,64}, S. J. Chen⁴², S. L. Chen⁴⁵, S. M. Chen⁶¹, T. Chen^{1,64}, X. R. Chen^{31,64}, X. T. Chen^{1,64}, Y. B. Chen^{1,58}, Y. Q. Chen³⁴, Z. J. Chen^{25,i}, Z. Y. Chen^{1,64}, S. K. Choi¹⁰, G. Cibinetto^{29A}, F. Cossio^{75C}, J. J. Cui⁵⁰, H. L. Dai^{1,58}, J. P. Dai⁷⁹, A. Dbeyssi¹⁸, R. E. de Boer³, D. Dedovich³⁶, C. Q. Deng⁷³, Z. Y. Deng¹, A. Denig³⁵, I. Denysenko³⁶, M. Destefanis^{75A,75C}, F. De Mori^{75A,75C}, B. Ding^{67,1}, X. X. Ding^{46,h}, Y. Ding⁴⁰, Y. Ding³⁴, J. Dong^{1,58}, L. Y. Dong^{1,64}, M. Y. Dong^{1,58,64}, X. Dong⁷⁷, M. C. Du¹, S. X. Du⁸¹, Y. Y. Duan⁵⁵, Z. H. Duan⁴², P. Egorov^{36,b}, Y. H. Fan⁴⁵, J. Fang⁵⁹, J. Fang^{1,58}, S. S. Fang^{1,64}, W. X. Fang¹, Y. Fang¹, Y. Q. Fang^{1,58}, R. Farinelli^{29A}, L. Fava^{75B,75C}, F. Feldbauer³, G. Felici^{28A}, C. Q. Feng^{72,58}, J. H. Feng⁵⁹, Y. T. Feng^{72,58}, M. Fritsch³, C. D. Fu¹, J. L. Fu⁶⁴, Y. W. Fu^{1,64}, H. Gao⁶⁴, X. B. Gao⁴¹, Y. N. Gao^{46,h}, Yang Gao^{72,58}, S. Garbolino^{75C}, I. Garzia^{29A,29B}, L. Ge⁸¹, P. T. Ge¹⁹, Z. W. Ge⁴², C. Geng⁵⁹, E. M. Gersabeck⁶⁸, A. Gilman⁷⁰, K. Goetzen¹³, L. Gong⁴⁰, W. X. Gong^{1,58}, W. Gradl³⁵, S. Gramigna^{29A,29B}, M. Greco^{75A,75C}, M. H. Gu^{1,58}, Y. T. Gu¹⁵, C. Y. Guan^{1,64}, A. Q. Guo^{31,64}, L. B. Guo⁴¹, M. J. Guo⁵⁰, R. P. Guo⁴⁹, Y. P. Guo^{12,g}, A. Guskov^{36,b}, J. Gutierrez²⁷, K. L. Han⁶⁴, T. T. Han¹, F. Hanisch³, X. Q. Hao¹⁹, F. A. Harris⁶⁶, K. K. He⁵⁵, K. L. He^{1,64}, F. H. Heinsius³, C. H. Heinz³⁵, Y. K. Heng^{1,58,64}, C. Herold⁶⁰, T. Holtmann³, P. C. Hong³⁴, G. Y. Hou^{1,64}, X. T. Hou^{1,64}, Y. R. Hou⁶⁴, Z. L. Hou¹, B. Y. Hu⁵⁹, H. M. Hu^{1,64}, J. F. Hu^{56,j}, S. L. Hu^{12,g}, T. Hu^{1,58,64}, Y. Hu¹, G. S. Huang^{72,58}, K. X. Huang⁵⁹, L. Q. Huang^{31,64}, X. T. Huang⁵⁰, Y. P. Huang¹⁰, Y. S. Huang⁵⁹, T. Hussain⁷⁴, F. Hölzken³, N. Hüsken³⁵, N. in der Wiesche⁶⁹, J. Jackson²⁷, S. Janchiv³², J. H. Jeong¹⁰, Q. Ji¹, Q. P. Ji¹⁹, W. Ji^{1,64}, X. B. Ji^{1,64}, X. L. Ji^{1,58}, Y. Y. Ji⁵⁰, X. Q. Jia⁵⁰, Z. K. Jia^{72,58}, D. Jiang^{1,64}, H. B. Jiang⁷⁷, P. C. Jiang^{46,h}, S. S. Jiang³⁹, T. J. Jiang¹⁶, X. S. Jiang^{1,58,64}, Y. J. Jiang⁶⁴, J. B. Jiao⁵⁰, J. K. Jiao³⁴, Z. Jiao²³, S. Jin⁴², Y. Jin⁶⁷, M. Q. Jing^{1,64}, X. M. Jing⁶⁴, T. Johansson⁷⁶, S. Kabana³³, N. Kalantar-Nayestanaki⁶⁵, X. L. Kang⁹, X. S. Kang⁴⁰, M. Kavatsyuk⁶⁵, B. C. Ke⁸¹, V. Khachatryan²⁷, A. Khoukaz⁶⁹, R. Kiuchi¹, O. B. Kolcu^{62A}, B. Kopf³, M. Kuessner³, X. Kui^{1,64}, N. Kumar²⁶, A. Kupsc^{44,76}, W. Kühn³⁷, J. J. Lane⁶⁸, L. Lavezzi^{75A,75C}, T. T. Lei^{72,58}, Z. H. Lei^{72,58}, M. Lellmann³⁵, T. Lenz³⁵, C. Li⁴⁷, C. Li⁴³, C. H. Li³⁹, Cheng Li^{72,58}, D. M. Li⁸¹, F. Li^{1,58}, G. Li¹, H. B. Li^{1,64}, H. J. Li¹⁹, H. N. Li^{56,j}, Hui Li⁴³, J. R. Li⁶¹, J. S. Li⁵⁹, K. Li¹, K. L. Li¹⁹, L. J. Li^{1,64}, L. K. Li¹, Lei Li⁴⁸, M. H. Li⁴³, P. R. Li^{38,k,l}, Q. M. Li^{1,64}, Q. X. Li⁵⁰, R. Li^{17,31}, S. X. Li¹², T. Li⁵⁰, W. D. Li^{1,64}, W. G. Li^{1,a}, X. Li^{1,64}, X. H. Li^{72,58}, X. L. Li⁵⁰, X. Y. Li^{1,64}, X. Z. Li⁵⁹, Y. G. Li^{46,h}, Z. J. Li⁵⁹, Z. Y. Li⁷⁹, C. Liang⁴², H. Liang^{1,64}, H. Liang^{72,58}, Y. F. Liang⁵⁴, Y. T. Liang^{31,64}, G. R. Liao¹⁴, Y. P. Liao^{1,64}, J. Libby²⁶, A. Limphirat⁶⁰, C. C. Lin⁵⁵, D. X. Lin^{31,64}, T. Lin¹, B. J. Liu¹, B. X. Liu⁷⁷, C. Liu³⁴, C. X. Liu¹, F. Liu¹, F. H. Liu⁵³, Feng Liu⁶, G. M. Liu^{56,j}, H. Liu^{38,k,l}, H. B. Liu¹⁵, H. H. Liu¹, H. M. Liu^{1,64}, Huihui Liu²¹, J. B. Liu^{72,58}, J. Y. Liu^{1,64}, K. Liu^{38,k,l}, K. Y. Liu⁴⁰, Ke Liu²², L. Liu^{72,58}, L. C. Liu⁴³, Lu Liu⁴³, M. H. Liu^{12,g}, P. L. Liu¹, Q. Liu⁶⁴, S. B. Liu^{72,58}, T. Liu^{12,g}, W. K. Liu⁴³, W. M. Liu^{72,58}, X. Liu^{38,k,l}, X. Liu³⁹, Y. Liu⁸¹, Y. Liu^{38,k,l}, Y. B. Liu⁴³, Z. A. Liu^{1,58,64}, Z. D. Liu⁹, Z. Q. Liu⁵⁰, X. C. Lou^{1,58,64}, F. X. Lu⁵⁹, H. J. Lu²³, J. G. Lu^{1,58}, X. L. Lu¹, Y. Lu⁷, Y. P. Lu^{1,58}, Z. H. Lu^{1,64}, C. L. Luo⁴¹, J. R. Luo⁵⁹, M. X. Luo⁸⁰, T. Luo^{12,g}, X. L. Luo^{1,58}, X. R. Lyu⁶⁴, Y. F. Lyu⁴³, F. C. Ma⁴⁰, H. Ma⁷⁹, H. L. Ma¹, J. L. Ma^{1,64}, L. L. Ma⁵⁰, L. R. Ma⁶⁷, M. M. Ma^{1,64}, Q. M. Ma¹, R. Q. Ma^{1,64}, T. Ma^{72,58}, X. T. Ma^{1,64}, X. Y. Ma^{1,58}, Y. Ma^{46,h}, Y. M. Ma³¹, F. E. Maas¹⁸, M. Maggiora^{75A,75C}, S. Malde⁷⁰, Y. J. Mao^{46,h}, Z. P. Mao¹, S. Marcello^{75A,75C}, Z. X. Meng⁶⁷, J. G. Messchendorp^{13,65}, G. Mezzadri^{29A}, H. Miao^{1,64}, T. J. Min⁴², R. E. Mitchell²⁷, X. H. Mo^{1,58,64}, B. Moses²⁷, N. Yu. Muchnoi^{4,c}, J. Muskalla³⁵, Y. Nefedov³⁶, F. Nerling^{18,e}, L. S. Nie²⁰, I. B. Nikolaev^{4,c}, Z. Ning^{1,58}, S. Nisar^{11,m}, Q. L. Niu^{38,k,l}, W. D. Niu⁵⁵, Y. Niu⁵⁰, S. L. Olsen⁶⁴, Q. Ouyang^{1,58,64}, S. Pacetti^{28B,28C}, X. Pan⁵⁵, Y. Pan⁵⁷, A. Pathak³⁴, Y. P. Pei^{72,58}, M. Pelizaeus³, H. P. Peng^{72,58}, Y. Y. Peng^{38,k,l}, K. Peters^{13,e}, J. L. Ping⁴¹, R. G. Ping^{1,64}, S. Plura³⁵, V. Prasad³³, F. Z. Qi¹, H. Qi^{72,58}, H. R. Qi⁶¹, M. Qi⁴², T. Y. Qi^{12,g}, S. Qian^{1,58}, W. B. Qian⁶⁴, C. F. Qiao⁶⁴, X. K. Qiao⁸¹, J. J. Qin⁷³, L. Q. Qin¹⁴, L. Y. Qin^{72,58}, X. P. Qin^{12,g}, X. S. Qin⁵⁰, Z. H. Qin^{1,58}, J. F. Qiu¹, Z. H. Qu⁷³, C. F. Redmer³⁵, K. J. Ren³⁹, A. Rivetti^{75C}, M. Rolo^{75C}, G. Rong^{1,64}, Ch. Rosner¹⁸, S. N. Ruan⁴³, N. Salone⁴⁴, A. Sarantsev^{36,d}, Y. Schelhaas³⁵, K. Schoenning⁷⁶, M. Scodeggio^{29A}, K. Y. Shan^{12,g}, W. Shan²⁴, X. Y. Shan^{72,58}, Z. J. Shang^{38,k,l}, J. F. Shangguan¹⁶, L. G. Shao^{1,64}, M. Shao^{72,58}, C. P. Shen^{12,g}, H. F. Shen^{1,8}, W. H. Shen⁶⁴, X. Y. Shen^{1,64}, B. A. Shi⁶⁴, H. Shi^{72,58}, H. C. Shi^{72,58}, J. L. Shi^{12,g}, J. Y. Shi¹, Q. Q. Shi⁵⁵, S. Y. Shi⁷³, X. Shi^{1,58}, J. J. Song¹⁹, T. Z. Song⁵⁹, W. M. Song^{34,1}, Y. J. Song^{12,g}, Y. X. Song^{46,h,n}, S. Sosio^{75A,75C}, S. Spataro^{75A,75C}, F. Stieler³⁵, S. S. Su⁴⁰, Y. J. Su⁶⁴, G. B. Sun⁷⁷, G. X. Sun¹, H. Sun⁶⁴, H. K. Sun¹, J. F. Sun¹⁹, K. Sun⁶¹, L. Sun⁷⁷, S. S. Sun^{1,64}, T. Sun^{51,f}, W. Y. Sun³⁴, Y. Sun⁹, Y. J. Sun^{72,58}, Y. Z. Sun¹, Z. Q. Sun^{1,64}, Z. T. Sun⁵⁰, C. J. Tang⁵⁴, G. Y. Tang¹, J. Tang⁵⁹, M. Tang^{72,58}, Y. A. Tang⁷⁷, L. Y. Tao⁷³, Q. T. Tao^{25,i}, M. Tat⁷⁰, J. X. Teng^{72,58}, V. Thoren⁷⁶, W. H. Tian⁵⁹, Y. Tian^{31,64}, Z. F. Tian⁷⁷, I. Uman^{62B}, Y. Wan⁵⁵, S. J. Wang⁵⁰, B. Wang¹, B. L. Wang⁶⁴, Bo Wang^{72,58}, D. Y. Wang^{46,h}, F. Wang⁷³, H. J. Wang^{38,k,l}, J. J. Wang⁷⁷, J. P. Wang⁵⁰, K. Wang^{1,58}, L. L. Wang¹, M. Wang⁵⁰, N. Y. Wang⁶⁴, S. Wang^{12,g}, S. Wang^{38,k,l}, T. Wang^{12,g}, T. J. Wang⁴³, W. Wang⁷³, W. Wang⁵⁹, W. P. Wang^{35,58,72,o}, X. Wang^{46,h}, X. F. Wang^{38,k,l}, X. J. Wang³⁹, X. L. Wang^{12,g}, X. N. Wang¹, Y. Wang⁶¹, Y. D. Wang⁴⁵, Y. F. Wang^{1,58,64}, Y. L. Wang¹⁹, Y. N. Wang⁴⁵, Y. Q. Wang¹, Yaqian Wang¹⁷, Yi Wang⁶¹, Z. Wang^{1,58}, Z. L. Wang⁷³, Z. Y. Wang^{1,64}, Ziyi Wang⁶⁴, D. H. Wei¹⁴, F. Weidner⁶⁹, S. P. Wen¹, Y. R. Wen³⁹, U. Wiedner³, G. Wilkinson⁷⁰, M. Wolke⁷⁶, L. Wollenberg³, C. Wu³⁹, J. F. Wu^{1,8}, L. H. Wu¹, L. J. Wu^{1,64}, X. Wu^{12,g}, X. H. Wu³⁴, Y. Wu^{72,58}, Y. H. Wu⁵⁵, Y. J. Wu³¹, Z. Wu^{1,58}, L. Xia^{72,58}, X. M. Xian³⁹, B. H. Xiang^{1,64}, T. Xiang^{46,h}, D. Xiao^{38,k,l}, G. Y. Xiao⁴², S. Y. Xiao¹, Y. L. Xiao^{12,g}, Z. J. Xiao⁴¹, C. Xie⁴², X. H. Xie^{46,h}, Y. Xie⁵⁰, Y. G. Xie^{1,58}, Y. H. Xie⁶, Z. P. Xie^{72,58}, T. Y. Xing^{1,64}, C. F. Xu^{1,64}, C. J. Xu⁵⁹, G. F. Xu¹, H. Y. Xu^{67,2,p}, M. Xu^{72,58}, Q. J. Xu¹⁶, Q. N. Xu³⁰, W. Xu¹, W. L. Xu⁶⁷, X. P. Xu⁵⁵, Y. Xu⁴⁰, Y. C. Xu⁷⁸, Z. S. Xu⁶⁴, F. Yan^{12,g}, L. Yan^{12,g}, W. B. Yan^{72,58},

W. C. Yan⁸¹, X. Q. Yan^{1,64}, H. J. Yang^{51,f}, H. L. Yang³⁴, H. X. Yang¹, T. Yang¹, Y. Yang^{12,g}, Y. F. Yang⁴³, Y. F. Yang^{1,64},
 Y. X. Yang^{1,64}, Z. W. Yang^{38,k,l}, Z. P. Yao⁵⁰, M. Ye^{1,58}, M. H. Ye⁸, J. H. Yin¹, Junhao Yin⁴³, Z. Y. You⁵⁹, B. X. Yu^{1,58,64},
 C. X. Yu⁴³, G. Yu^{1,64}, J. S. Yu^{25,i}, M. C. Yu⁴⁰, T. Yu⁷³, X. D. Yu^{46,h}, Y. C. Yu⁸¹, C. Z. Yuan^{1,64}, J. Yuan³⁴, J. Yuan⁴⁵,
 L. Yuan², S. C. Yuan^{1,64}, Y. Yuan^{1,64}, Z. Y. Yuan⁵⁹, C. X. Yue³⁹, A. A. Zafar⁷⁴, F. R. Zeng⁵⁰, S. H. Zeng^{63A,63B,63C,63D},
 X. Zeng^{12,g}, Y. Zeng^{25,i}, Y. J. Zeng⁵⁹, Y. J. Zeng^{1,64}, X. Y. Zhai³⁴, Y. C. Zhai⁵⁰, Y. H. Zhan⁵⁹, A. Q. Zhang^{1,64},
 B. L. Zhang^{1,64}, B. X. Zhang¹, D. H. Zhang⁴³, G. Y. Zhang¹⁹, H. Zhang^{72,58}, H. Zhang⁸¹, H. C. Zhang^{1,58,64}, H. H. Zhang⁵⁹,
 H. H. Zhang³⁴, H. Q. Zhang^{1,58,64}, H. R. Zhang^{72,58}, H. Y. Zhang^{1,58}, J. Zhang⁸¹, J. Zhang⁵⁹, J. J. Zhang⁵², J. L. Zhang²⁰,
 J. Q. Zhang⁴¹, J. S. Zhang^{12,g}, J. W. Zhang^{1,58,64}, J. X. Zhang^{38,k,l}, J. Y. Zhang¹, J. Z. Zhang^{1,64}, Jianyu Zhang⁶⁴,
 L. M. Zhang⁶¹, Lei Zhang⁴², P. Zhang^{1,64}, Q. Y. Zhang³⁴, R. Y. Zhang^{38,k,l}, S. H. Zhang^{1,64}, Shulei Zhang^{25,i}, X. D. Zhang⁴⁵,
 X. M. Zhang¹, X. Y. Zhang⁴⁰, X. Y. Zhang⁵⁰, Y. Zhang⁷³, Y. Zhang¹, Y. T. Zhang⁸¹, Y. H. Zhang^{1,58}, Y. M. Zhang³⁹,
 Yan Zhang^{72,58}, Z. D. Zhang¹, Z. H. Zhang¹, Z. L. Zhang³⁴, Z. Y. Zhang⁷⁷, Z. Y. Zhang⁴³, Z. Z. Zhang⁴⁵, G. Zhao¹,
 J. Y. Zhao^{1,64}, J. Z. Zhao^{1,58}, L. Zhao¹, Lei Zhao^{72,58}, M. G. Zhao⁴³, N. Zhao⁷⁹, R. P. Zhao⁶⁴, S. J. Zhao⁸¹, Y. B. Zhao^{1,58},
 Y. X. Zhao^{31,64}, Z. G. Zhao^{72,58}, A. Zhemchugov^{36,b}, B. Zheng⁷³, B. M. Zheng³⁴, J. P. Zheng^{1,58}, W. J. Zheng^{1,64},
 Y. H. Zheng⁶⁴, B. Zhong⁴¹, X. Zhong⁵⁹, H. Zhou⁵⁰, J. Y. Zhou³⁴, L. P. Zhou^{1,64}, S. Zhou⁶, X. Zhou⁷⁷, X. K. Zhou⁶,
 X. R. Zhou^{72,58}, X. Y. Zhou³⁹, Y. Z. Zhou^{12,g}, Z. C. Zhou²⁰, A. N. Zhu⁶⁴, J. Zhu⁴³, K. Zhu¹, K. J. Zhu^{1,58,64}, K. S. Zhu^{12,g},
 L. Zhu³⁴, L. X. Zhu⁶⁴, S. H. Zhu⁷¹, T. J. Zhu^{12,g}, W. D. Zhu⁴¹, Y. C. Zhu^{72,58}, Z. A. Zhu^{1,64}, J. H. Zou¹, J. Zu^{72,58}

(BESIII Collaboration)

¹ Institute of High Energy Physics, Beijing 100049, People's Republic of China

² Beihang University, Beijing 100191, People's Republic of China

³ Bochum Ruhr-University, D-44780 Bochum, Germany

⁴ Budker Institute of Nuclear Physics SB RAS (BINP), Novosibirsk 630090, Russia

⁵ Carnegie Mellon University, Pittsburgh, Pennsylvania 15213, USA

⁶ Central China Normal University, Wuhan 430079, People's Republic of China

⁷ Central South University, Changsha 410083, People's Republic of China

⁸ China Center of Advanced Science and Technology, Beijing 100190, People's Republic of China

⁹ China University of Geosciences, Wuhan 430074, People's Republic of China

¹⁰ Chung-Ang University, Seoul, 06974, Republic of Korea

¹¹ COMSATS University Islamabad, Lahore Campus, Defence Road, Off Raiwind Road, 54000 Lahore, Pakistan

¹² Fudan University, Shanghai 200433, People's Republic of China

¹³ GSI Helmholtzcentre for Heavy Ion Research GmbH, D-64291 Darmstadt, Germany

¹⁴ Guangxi Normal University, Guilin 541004, People's Republic of China

¹⁵ Guangxi University, Nanning 530004, People's Republic of China

¹⁶ Hangzhou Normal University, Hangzhou 310036, People's Republic of China

¹⁷ Hebei University, Baoding 071002, People's Republic of China

¹⁸ Helmholtz Institute Mainz, Staudinger Weg 18, D-55099 Mainz, Germany

¹⁹ Henan Normal University, Xinxiang 453007, People's Republic of China

²⁰ Henan University, Kaifeng 475004, People's Republic of China

²¹ Henan University of Science and Technology, Luoyang 471003, People's Republic of China

²² Henan University of Technology, Zhengzhou 450001, People's Republic of China

²³ Huangshan College, Huangshan 245000, People's Republic of China

²⁴ Hunan Normal University, Changsha 410081, People's Republic of China

²⁵ Hunan University, Changsha 410082, People's Republic of China

²⁶ Indian Institute of Technology Madras, Chennai 600036, India

²⁷ Indiana University, Bloomington, Indiana 47405, USA

²⁸ INFN Laboratori Nazionali di Frascati, (A)INFN Laboratori Nazionali di Frascati, I-00044, Frascati, Italy; (B)INFN

Sezione di Perugia, I-06100, Perugia, Italy; (C)University of Perugia, I-06100, Perugia, Italy

²⁹ INFN Sezione di Ferrara, (A)INFN Sezione di Ferrara, I-44122, Ferrara, Italy; (B)University of Ferrara, I-44122, Ferrara, Italy

³⁰ Inner Mongolia University, Hohhot 010021, People's Republic of China

³¹ Institute of Modern Physics, Lanzhou 730000, People's Republic of China

³² Institute of Physics and Technology, Peace Avenue 54B, Ulaanbaatar 13330, Mongolia

³³ Instituto de Alta Investigación, Universidad de Tarapacá, Casilla 7D, Arica 1000000, Chile

³⁴ Jilin University, Changchun 130012, People's Republic of China

³⁵ Johannes Gutenberg University of Mainz, Johann-Joachim-Becher-Weg 45, D-55099 Mainz, Germany

³⁶ Joint Institute for Nuclear Research, 141980 Dubna, Moscow region, Russia

³⁷ Justus-Liebig-Universität Giessen, II. Physikalisches Institut, Heinrich-Buff-Ring 16, D-35392 Giessen, Germany

³⁸ Lanzhou University, Lanzhou 730000, People's Republic of China

³⁹ Liaoning Normal University, Dalian 116029, People's Republic of China

⁴⁰ Liaoning University, Shenyang 110036, People's Republic of China

⁴¹ Nanjing Normal University, Nanjing 210023, People's Republic of China

⁴² Nanjing University, Nanjing 210093, People's Republic of China

⁴³ Nankai University, Tianjin 300071, People's Republic of China

- ⁴⁴ National Centre for Nuclear Research, Warsaw 02-093, Poland
- ⁴⁵ North China Electric Power University, Beijing 102206, People's Republic of China
- ⁴⁶ Peking University, Beijing 100871, People's Republic of China
- ⁴⁷ Qufu Normal University, Qufu 273165, People's Republic of China
- ⁴⁸ Renmin University of China, Beijing 100872, People's Republic of China
- ⁴⁹ Shandong Normal University, Jinan 250014, People's Republic of China
- ⁵⁰ Shandong University, Jinan 250100, People's Republic of China
- ⁵¹ Shanghai Jiao Tong University, Shanghai 200240, People's Republic of China
- ⁵² Shanxi Normal University, Linfen 041004, People's Republic of China
- ⁵³ Shanxi University, Taiyuan 030006, People's Republic of China
- ⁵⁴ Sichuan University, Chengdu 610064, People's Republic of China
- ⁵⁵ Soochow University, Suzhou 215006, People's Republic of China
- ⁵⁶ South China Normal University, Guangzhou 510006, People's Republic of China
- ⁵⁷ Southeast University, Nanjing 211100, People's Republic of China
- ⁵⁸ State Key Laboratory of Particle Detection and Electronics, Beijing 100049, Hefei 230026, People's Republic of China
- ⁵⁹ Sun Yat-Sen University, Guangzhou 510275, People's Republic of China
- ⁶⁰ Suranaree University of Technology, University Avenue 111, Nakhon Ratchasima 30000, Thailand
- ⁶¹ Tsinghua University, Beijing 100084, People's Republic of China
- ⁶² Turkish Accelerator Center Particle Factory Group, (A)Istinye University, 34010, Istanbul, Turkey; (B)Near East University, Nicosia, North Cyprus, 99138, Mersin 10, Turkey
- ⁶³ University of Bristol, (A)H H Wills Physics Laboratory; (B)Tyndall Avenue; (C)Bristol; (D)BS8 1TL
- ⁶⁴ University of Chinese Academy of Sciences, Beijing 100049, People's Republic of China
- ⁶⁵ University of Groningen, NL-9747 AA Groningen, The Netherlands
- ⁶⁶ University of Hawaii, Honolulu, Hawaii 96822, USA
- ⁶⁷ University of Jinan, Jinan 250022, People's Republic of China
- ⁶⁸ University of Manchester, Oxford Road, Manchester, M13 9PL, United Kingdom
- ⁶⁹ University of Muenster, Wilhelm-Klemm-Strasse 9, 48149 Muenster, Germany
- ⁷⁰ University of Oxford, Keble Road, Oxford OX13RH, United Kingdom
- ⁷¹ University of Science and Technology Liaoning, Anshan 114051, People's Republic of China
- ⁷² University of Science and Technology of China, Hefei 230026, People's Republic of China
- ⁷³ University of South China, Hengyang 421001, People's Republic of China
- ⁷⁴ University of the Punjab, Lahore-54590, Pakistan
- ⁷⁵ University of Turin and INFN, (A)University of Turin, I-10125, Turin, Italy; (B)University of Eastern Piedmont, I-15121, Alessandria, Italy; (C)INFN, I-10125, Turin, Italy
- ⁷⁶ Uppsala University, Box 516, SE-75120 Uppsala, Sweden
- ⁷⁷ Wuhan University, Wuhan 430072, People's Republic of China
- ⁷⁸ Yantai University, Yantai 264005, People's Republic of China
- ⁷⁹ Yunnan University, Kunming 650500, People's Republic of China
- ⁸⁰ Zhejiang University, Hangzhou 310027, People's Republic of China
- ⁸¹ Zhengzhou University, Zhengzhou 450001, People's Republic of China
- ^a Deceased
- ^b Also at the Moscow Institute of Physics and Technology, Moscow 141700, Russia
- ^c Also at the Novosibirsk State University, Novosibirsk, 630090, Russia
- ^d Also at the NRC "Kurchatov Institute", PNPI, 188300, Gatchina, Russia
- ^e Also at Goethe University Frankfurt, 60323 Frankfurt am Main, Germany
- ^f Also at Key Laboratory for Particle Physics, Astrophysics and Cosmology, Ministry of Education; Shanghai Key Laboratory for Particle Physics and Cosmology; Institute of Nuclear and Particle Physics, Shanghai 200240, People's Republic of China
- ^g Also at Key Laboratory of Nuclear Physics and Ion-beam Application (MOE) and Institute of Modern Physics, Fudan University, Shanghai 200443, People's Republic of China
- ^h Also at State Key Laboratory of Nuclear Physics and Technology, Peking University, Beijing 100871, People's Republic of China
- ⁱ Also at School of Physics and Electronics, Hunan University, Changsha 410082, China
- ^j Also at Guangdong Provincial Key Laboratory of Nuclear Science, Institute of Quantum Matter, South China Normal University, Guangzhou 510006, China
- ^k Also at MOE Frontiers Science Center for Rare Isotopes, Lanzhou University, Lanzhou 730000, People's Republic of China
- ^l Also at Lanzhou Center for Theoretical Physics, Lanzhou University, Lanzhou 730000, People's Republic of China
- ^m Also at the Department of Mathematical Sciences, IBA, Karachi 75270, Pakistan
- ⁿ Also at Ecole Polytechnique Federale de Lausanne (EPFL), CH-1015 Lausanne, Switzerland
- ^o Also at Helmholtz Institute Mainz, Staudinger Weg 18, D-55099 Mainz, Germany
- ^p Also at School of Physics, Beihang University, Beijing 100191, China

We study the electromagnetic Dalitz decay $J/\psi \rightarrow e^+e^-\pi^0$ using $(10087 \pm 44) \times 10^6$ J/ψ events collected by the BESIII detector. The di-electron-invariant-mass dependent transition form factor

of this decay is explored for the first time. A significant resonant structure corresponding to the ρ/ω resonance is observed, which cannot be described by existing theoretical models, due to contributions from the isospin-conserving $J/\psi \rightarrow \rho\pi^0$ and isospin-violating $J/\psi \rightarrow \omega\pi^0$ decays. The observed ρ - ω interference is consistent with that of the pion form factor but features a relatively narrow ρ peak. By taking into account the contribution of this resonant structure, the branching fraction of $J/\psi \rightarrow e^+e^-\pi^0$ in the full e^+e^- invariant mass spectrum range is also measured for the first time to be $(8.06 \pm 0.31(\text{stat}) \pm 0.38(\text{syst})) \times 10^{-7}$, which is two times larger than the prediction of the Vector Meson Dominance model due to the observed resonant contribution of ρ/ω resonances.

An electromagnetic (EM) Dalitz decay [1] proceeds via conversion of an off-shell photon into a lepton pair [2]. The q^2 -dependent transition form factor (TFF), where q^2 is the four-momentum transfer squared and is equal to the square of the di-lepton invariant mass [3], provides access to possible deviations from the standard point-like prediction of quantum electrodynamics (QED) [2]. Thus, a TFF is a sensitive tool to probe the inner structure of the involved hadrons. Within the vector meson dominance (VMD) model [4], the TFF describes the interaction of the photons with hadrons via an intermediate vector meson V' in the time-like region [5]. These TFFs are important inputs in the calculation of the hadronic light-by-light contribution of the anomalous magnetic moment of the muon [6], $a_\mu = (g_\mu - 2)/2$, which is of great interest in precision tests of the Standard Model [7–9] and EM Dalitz decay rates [2].

Most measured EM Dalitz decays of the light unflavored vector mesons ρ , ω , and ϕ [10, 11] are compatible with the VMD assumption [2]. However, some of the experimental results, such as $\omega \rightarrow \mu^+\mu^-\pi^0$, indicate large deviations [12, 13] that are difficult to understand with existing theoretical models [14]. A similar situation has recently also appeared in the EM Dalitz decays of charmonium vector mesons, such as in recent measurements of the EM Dalitz decays $J/\psi \rightarrow e^+e^-P$ ($P = \pi^0, \eta, \eta'$) [15, 16]. The measured branching fractions of $J/\psi \rightarrow e^+e^-\eta/\eta'$ agree well with the VMD prediction [17]. However, the branching fraction of $J/\psi \rightarrow e^+e^-\pi^0$, $(7.56 \pm 1.32 \pm 0.50) \times 10^{-7}$ [15], measured by BESIII for di-electron invariant masses ($m_{e^+e^-}$) less than $0.4 \text{ GeV}/c^2$ using 225 million J/ψ events, deviates by more than three standard deviations from the predictions based on the VMD model [17], an effective Lagrangian-based analysis [18], and dispersion theory [19]. The latter two models [18, 19] also take into account the contribution of the intermediate light vector meson ρ . This discrepancy may disappear after considering the resonant contributions from the isospin conserving decay $J/\psi \rightarrow \rho\pi^0$ and the isospin violating decays $J/\psi \rightarrow \omega/\phi\pi^0$ [20]. However, the well-known ρ - ω interference, as proposed by Glashow [21], may also appear in these decays, as discussed in Ref. [22].

An experimental study of ρ - ω interference is desirable for testing charge symmetry violation (CSV) [23–25], quantum chromodynamics sum rules (QCDSR) [26, 27], chiral perturbation theory (ChPT) [28, 29], and hidden

local symmetry (HLS) [30, 31]. The interference has been well-established in the measurement of the pionic cross-section $\sigma(e^+e^- \rightarrow \pi^+\pi^-)$ [32–34]. The contribution of ρ - ω interference has an impact on the measurements of the isospin-violating $\omega \rightarrow \pi^+\pi^-$ decay rate [32], the running QED coupling constant [35], and the evaluation of the 2π contribution to the hadronic vacuum polarization part of a_μ [32–34]. An investigation of ρ - ω interference in a purely EM channel was previously reported via the photoproduction of electron-positron pairs off carbon [36], beryllium [37], and hydrogen [36] targets, but the phases of the interference were found to be different from those corresponding to pionic channels, such as $e^+e^- \rightarrow \pi^+\pi^-$ [32–34]. This discrepancy may be resolved by investigating the ρ - ω interference in the intermediate resonances of $J/\psi \rightarrow e^+e^-\pi^0$. The same J/ψ decay also tests various theoretical models [2, 17–19], could improve the accuracy of $J/\psi \rightarrow V'\pi^0$ ($V' = \rho, \omega$) decay rates [20], and probes G-parity violation [22]. This Letter reports the first measurement of the q^2 -dependent TFF and an improved measurement of the branching fraction of the EM Dalitz decay $J/\psi \rightarrow e^+e^-\pi^0$ in the full $m_{e^+e^-}$ spectrum using a data sample of $(10087 \pm 44) \times 10^6$ J/ψ events collected by the BESIII detector.

BESIII is a general purpose detector operating at the e^+e^- BEPCII collider, and is described in more detail in Ref. [39]. Monte Carlo (MC) simulated events based on GEANT4 [40] are used to study the detection efficiency, to optimize the event selection criteria, and to investigate potential backgrounds. Time-dependent effects, such as beam-related backgrounds and detector running conditions during the data collection period, are included in the MC simulation. An inclusive MC sample of 10 billion events of generic J/ψ decays, generated by EVTGEN [41] for known decay modes with branching fractions quoted in Ref. [20] and by LUNDCHARM [42] for unknown decay modes, is used for background studies. The signal MC sample is generated using EVTGEN [41] according to a Lorentz-invariant amplitude [43], where the TFF function is directly extracted from the data while taking into account the contribution of intermediate V' resonances in the decay as described below. Furthermore, another signal MC sample containing only the non-resonant contribution of the $J/\psi \rightarrow e^+e^-\pi^0$ decay is also generated with the same model by setting the TFF to unity. This is also referred to as the point-like process and is used to optimize the event selection criteria and study the $m_{e^+e^-}$

dependent TFF.

We select events of interest by requiring two oppositely charged tracks and at least two good photon candidates. Charged tracks are reconstructed from the ionization signals measured by the main drift chamber (MDC). The point of closest approach of each charged track to the e^+e^- interaction point (IP) is required to be within ± 10.0 cm along the z -axis, which is the symmetry axis of the MDC and within ± 1.0 cm in the plane perpendicular to the z -axis. Each charged track is required to be within the active region of the MDC $|\cos\theta| < 0.93$, where θ is the angle between the direction of a charged track and the z -axis. The PID algorithm, based on the specific energy loss dE/dx and information from the time-of-flight (TOF) system and the electromagnetic calorimeter (EMC), forms a likelihood $\mathcal{L}(h)$, where h is a particle hypothesis of e^\pm , π^\pm or K^\pm charged tracks. Both of the charged tracks are identified as e^\pm by requiring $\mathcal{L}(e^\pm) > \mathcal{L}(\pi^\pm)$ and $\mathcal{L}(e^\pm) > \mathcal{L}(K^\pm)$. We further suppress pion contamination by requiring $E/p_{e^\pm} > 0.8$ c for those charged tracks with momenta larger than 0.25 GeV/ c , where E is the energy deposited in the EMC and p_{e^\pm} is the momentum measured by the MDC.

Showers are reconstructed from clusters of energy deposited in the EMC crystals. The shower energy of each photon is required to be greater than 25 MeV in the barrel region ($|\cos\theta| < 0.8$) or 50 MeV in the end-cap regions ($0.86 < |\cos\theta| < 0.92$). In order to improve the reconstruction efficiency and energy resolution, the energy deposited in the nearby TOF is taken into account. Showers poorly reconstructed in the transition region between the barrel and end-cap are discarded. In order to suppress the electronic noise and energy deposition unrelated to the events, the photon time as given by the EMC is required to be less than 700 ns after the collision.

A vertex fit is performed to the two charged tracks to ensure that they originate from a common vertex point. In order to improve the π^0 mass resolution, a four-constraint (4C) kinematic fit imposing energy and momentum conservation is implemented for the selected charged tracks and the two good photon candidates under the hypothesis of $J/\psi \rightarrow e^+e^-\gamma\gamma$. If there are more than two good photon candidates in the event, all $\gamma\gamma$ combinations are tested and the pair that gives the lowest value of chi-square of the kinematic fit, χ_{4C}^2 , is selected. To suppress peaking background from $J/\psi \rightarrow \gamma\pi^0\pi^0$, where one of the π^0 candidates decays in its Dalitz decay mode $\pi^0 \rightarrow \gamma e^+e^-$, the χ_{4C}^2 is further required to be less than 100. Candidate events are required to have a diphoton invariant mass, $m_{\gamma\gamma}$, within the range [0.09, 0.18] GeV/ c^2 .

The MC studies indicate that the background is dominated by the radiative Bhabha process $e^+e^- \rightarrow \gamma e^+e^-$, especially in the high $m_{e^+e^-}$ region, due to its large cross-section. The background contributes a smooth distribution in the $m_{\gamma\gamma}$ spectrum. This non-peaking background

is suppressed by requiring the momentum of the selected e^\pm to be less than 1.45 GeV/ c and the energy of the low energy photon (E_{γ_2}) used to reconstruct the π^0 candidate to be larger than 0.14 GeV.

At this stage, the background is dominated by events from the radiative decay $J/\psi \rightarrow \gamma\pi^0$, in which the radiative photon converts into an e^+e^- pair in the detector material. This background produces a π^0 peak in the $m_{\gamma\gamma}$ spectrum, namely a peaking background. To suppress this background, a γ conversion finder algorithm [44] is imposed. The distance from the vertex point of the e^+e^- pair to the origin in the $x-y$ plane is defined as $\delta_{xy} = \sqrt{R_x^2 + R_y^2}$, where R_x and R_y are the coordinates of the reconstructed vertex point along the x and y directions, respectively. In the distribution of R_y versus R_x , the signal events from $J/\psi \rightarrow e^+e^-\pi^0$ accumulate in the center of the circle, and the background events from $J/\psi \rightarrow \gamma\pi^0$ accumulate in the circles with radii of 3.5 cm and 6.5 cm corresponding to the positions of the beam pipe and inner wall of the MDC, respectively, as described in Fig. 1 of Ref. [49]. A requirement of $\delta_{xy} < 2$ cm is imposed, which eliminates around 98% of the γ conversion background with a loss of about 20% of the signal events.

The two-photon process [45], which proceeds via the interaction of two virtual photons emitted by the lepton pair in an e^+e^- collider experiment, can produce an even C -parity state of the pseudoscalar meson. In the case of π^0 production, the corresponding process $e^+e^- \rightarrow e^+e^-\pi^0$ has the same final state as the signal of interest. It therefore contributes as a peaking background in the $m_{\gamma\gamma}$ spectrum. An independent sample of $\psi(3770)$ data with an integrated luminosity of 2.93 fb $^{-1}$ [33], which is away from J/ψ resonance and is assumed to provide a pure sample of $e^+e^- \rightarrow e^+e^-\pi^0$ events, is used to study this background. The two-photon background events mainly accumulate in the bands of $\cos\theta(e^+) > 0.8$ or $\cos\theta(e^-) < -0.8$, away from the signal that accumulates around $\cos\theta(e^+) = \cos\theta(e^-)$, as described in Ref. [46]. This background is suppressed by requiring $\cos\theta(e^+) < 0.8$ and $\cos\theta(e^-) > -0.8$. After applying this selection criterion, the number of two-photon events in the J/ψ data sample is evaluated as $N_{J/\psi} = f \cdot N_{\psi(3770)}$, where $N_{\psi(3770)}$ is the number of signal events in the $\psi(3770)$ data sample surviving the same selection criteria, and $f = \frac{\mathcal{L}_{J/\psi}}{\mathcal{L}_{\psi(3770)}} \cdot \frac{\sigma_{J/\psi}}{\sigma_{\psi(3770)}} \cdot \frac{\epsilon_{J/\psi}}{\epsilon_{\psi(3770)}} = 3.59 \pm 0.02$ is the scale factor between the two data samples X ($X = J/\psi$ and $\psi(3770)$), which takes into account the integrated luminosities \mathcal{L}_X , the cross-sections σ_X and the efficiencies ϵ_X [45]. The detection efficiency ratio $\frac{\epsilon_{J/\psi}}{\epsilon_{\psi(3770)}}$ and cross-section ratio $\frac{\sigma_{J/\psi}}{\sigma_{\psi(3770)}}$ are evaluated to be 4.03 ± 0.02 and 0.878 ± 0.001 , respectively, with the EKHARA generator [47]. The value of $\epsilon_{\psi(3770)}$ is reduced due to the selection criteria on the e^\pm momentum, as described above. The yield $N_{\psi(3770)} = 27.9 \pm 13.6$ is

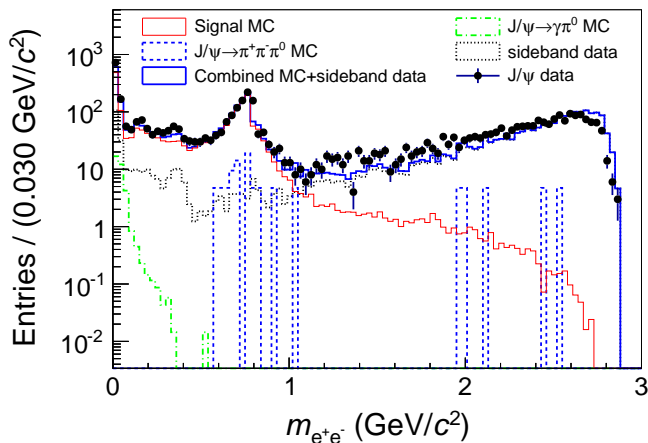


FIG. 1. Distribution of $m_{e^+e^-}$ for selected events in data (black dots with error bars), signal MC (red histogram), $J/\psi \rightarrow \gamma\pi^0$ MC (green long-dashed dotted histogram), $J/\psi \rightarrow \pi^+\pi^-\pi^0$ (blue dashed histogram), sideband data (black dotted histogram), and combined MC and sideband data (solid blue histogram). The signal MC sample includes the contributions of both resonant and non-resonant components from $J/\psi \rightarrow e^+e^-\pi^0$.

obtained by performing an extended maximum likelihood (ML) fit to the $m_{\gamma\gamma}$ spectrum of events selected from the $\psi(3770)$ data sample. Therefore, the expected number of two-photon events for the J/ψ data sample is estimated to be 100.0 ± 48.8 .

Figure 1 shows the $m_{e^+e^-}$ distribution for surviving events from the data, signal MC, and the remaining background processes. The contribution from the non-peaking background is dominated by the radiative Bhabha process. This background is evaluated using events in the π^0 sideband regions, defined as $[0.02, 0.08]$ and $[0.19, 0.30]$ GeV/c^2 . The peaking background is dominated by the decay $J/\psi \rightarrow \pi^+\pi^-\pi^0$ (99.4 ± 3.8 events including the ρ resonance and due to the π^\pm mis-identified to be e^\pm), $J/\psi \rightarrow \gamma\pi^0$ (35.2 ± 1.7 events), $J/\psi \rightarrow \gamma\pi^0\pi^0$ (2.8 ± 0.2 events), and $J/\psi \rightarrow \omega\pi^0$, $\omega \rightarrow \pi^+\pi^-$ (0.5 ± 0.1 events), where uncertainties include statistical and systematic uncertainties. The expected numbers of background events are evaluated using large MC samples normalized to their corresponding branching fractions quoted from Ref. [20]. The simulated events are also used for evaluating the resonant contributions of $J/\psi \rightarrow V'\pi^0$, $V' \rightarrow e^+e^-$, considered to be part of the signal mode, and are 690.0 ± 86.6 events for $\rho \rightarrow e^+e^-$ and 85.5 ± 9.8 for $\omega \rightarrow e^+e^-$, normalized to the branching fractions in Ref. [20].

The signal yield is determined by performing an extended ML fit to the $m_{\gamma\gamma}$ spectrum of the selected candidate events in data. In the fit, the probability density function (PDF) of the signal is described by the MC simulated shape convolved with a Gaussian func-

tion (with free parameters), which compensates for the resolution difference between data and MC simulation. The PDF of the non-peaking background is described by a first-order Chebyshev polynomial function with free parameters. The fit is shown in Fig. 2 over the full $m_{e^+e^-}$ spectrum, and yields $N_{\text{sig}}^{\text{data}} = 2347 \pm 66$ events, including both signal and peaking background contributions. By subtracting the contributions from the decays $J/\psi \rightarrow \pi^+\pi^-\pi^0$, $J/\psi \rightarrow \gamma\pi^0$, $J/\psi \rightarrow \gamma\pi^0\pi^0$, $J/\psi \rightarrow \omega(\rightarrow \pi^+\pi^-\pi^0)$, $J/\psi \rightarrow \omega\pi^0\pi^0$, and the two-photon process $e^+e^- \rightarrow e^+e^-\pi^0$, estimated above, the net signal yield is determined to be $N_{\text{sig}} = 2108.9 \pm 82.2$, where the total uncertainties on the peaking backgrounds are added in quadrature with the statistical uncertainty on N_{sig} . The obtained N_{sig} includes the contributions of the non-resonant $J/\psi \rightarrow e^+e^-\pi^0$ and the resonant $J/\psi \rightarrow \rho/\omega\pi^0$, $\rho/\omega \rightarrow e^+e^-$ decays. The branching fraction of $J/\psi \rightarrow e^+e^-\pi^0$ is calculated to be $(8.06 \pm 0.31 \pm 0.38) \times 10^{-7}$, where the first uncertainty is statistical and the second is systematic as described below and in the supplemental material [49], by the following formula,

$$\mathcal{B}(J/\psi \rightarrow e^+e^-\pi^0) = \frac{N_{\text{sig}}}{N_{J/\psi} \cdot \epsilon \cdot \mathcal{B}(\pi^0 \rightarrow \gamma\gamma)}. \quad (1)$$

Here, $\epsilon = 26.3\%$ is the signal selection efficiency obtained from a signal MC sample, depicted in Fig. 1, generated using the fitted TFF function of Eq. 2 with a pole mass $\Lambda = 3.686$ GeV/c^2 , as described below to take into account both the resonant and non-resonant contributions of $J/\psi \rightarrow e^+e^-\pi^0$. The $\mathcal{B}(\pi^0 \rightarrow \gamma\gamma)$ is the branching fraction of $\pi^0 \rightarrow \gamma\gamma$ from Ref. [20] and $N_{J/\psi} = (10087 \pm 44) \times 10^6$ is the total number of J/ψ events from Ref. [48].

To avoid the observed ρ/ω contributions, the branching fraction of $J/\psi \rightarrow e^+e^-\pi^0$ for $m_{e^+e^-} < 0.3$ GeV/c^2 is determined to be $(4.41 \pm 0.18 \pm 0.21) \times 10^{-7}$, which is consistent with the VMD prediction from Ref. [17], using a similar fit procedure detailed in Ref. [49]. Thus, this agreement and disappearance of the previously claimed discrepancy [15] are valid only for events with quasi-real photons, i.e., for small $m_{e^+e^-}$. However, our analysis shows that VMD [17] underestimates the total branching fraction by approximately a factor of two, as it does not include contributions from the ρ/ω resonances.

The q^2 -dependent TFF of $J/\psi \rightarrow e^+e^-$ is studied by comparing the measured differential branching fraction to that of the point-like prediction. The signal yield in each $m_{e^+e^-}$ bin is extracted by the same ML fit on the $m_{\gamma\gamma}$ distribution as described above. The corresponding detection efficiency (ϵ) is calculated with a signal MC sample generated under the point-like assumption that the TFF is equal to unity. In order to handle background from radiative Bhabha events, the fit is performed with various $m_{e^+e^-}$ bin widths with a total of 30 $m_{e^+e^-}$ points

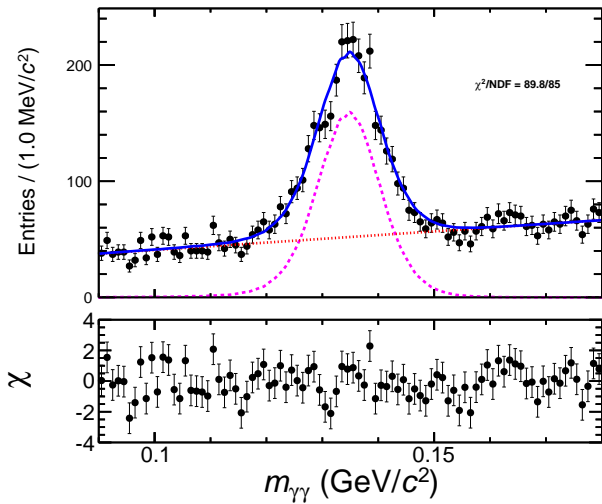


FIG. 2. The fit to the $m_{\gamma\gamma}$ distribution (top) together with the normalized fit residuals (bottom). The black dots with error bars are data, the pink dashed curve the signal, the red dotted curve the non-peaking background, and the blue solid curve the total projection.

detailed in Table 1 of Ref. [49]. The obtained distribution of the differential branching fractions, calculated after subtracting the aforementioned peaking backgrounds (except the background from the two-photon process) using the signal yields in each bin of $m_{e^+e^-}$, deviates from the point-like model prediction obtained from the formula in Eq. (3.4) of Ref. [2], the effective Lagrangian-based analysis [18], and dispersion theory [19], as shown in Fig. 3. An interference between the ρ and ω is observed for the first time in the $J/\psi \rightarrow e^+e^-\pi^0$ decay, which cannot be explained by the existing theoretical models of effective Lagrangian-based analysis [18] and dispersion theory [19].

The TFF ($|F_{J/\psi\pi^0}(q^2)|^2$) in each $m_{e^+e^-}$ bin, shown in Table (1) of Ref. [49], is calculated as the ratio of the corrected signal yield to the prediction of the point-like model integrated over the $m_{e^+e^-}$ bin interval, as shown in Fig. 4. To achieve a unity value of the TFF at $q^2 = 0$, the $|F_{J/\psi\pi^0}(q^2)|^2$ versus $m_{e^+e^-}$ data is normalized using the central value of the TFF from the first $m_{e^+e^-}$ bin. To study the observed $\rho - \omega$ interference, the TFF is fitted using the Gounaris-Sakurai function ($F_{J/\psi\pi^0}^{\text{GS}}(q^2)$) [50], described in detail in Ref. [34] and previously used by both the BESIII [33] and BaBar [34] experiments in the measurement of the $e^+e^- \rightarrow \pi^+\pi^-$ cross-section in the ρ/ω mass region, with and without including the contributions of the ρ' , ρ'' and ρ''' resonances. The best agreement between data and fit is achieved when these higher-order ρ resonances are excluded. The TFF versus $m_{e^+e^-}$ data in the full $m_{e^+e^-}$ range is fitted with the following function to take into account both the resonant and non-resonant contributions,

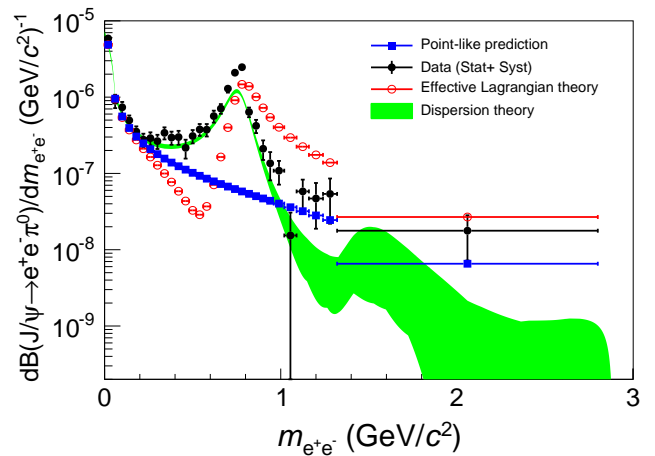


FIG. 3. The differential branching fraction for $J/\psi \rightarrow e^+e^-\pi^0$ normalized to the bin size versus $m_{e^+e^-}$ for data (black dots with error bars, including the statistical and systematic uncertainties combined in quadrature), the point-like prediction (blue squares with error bars), the effective Lagrangian theory prediction [18] (red circles with error bars), and the dispersion theory [19] prediction (green band).

$$F_{J/\psi\pi^0}(q^2) = F_{J/\psi\pi^0}^{\text{GS}}(q^2) + A_\Lambda \frac{1}{1 - q^2/\Lambda^2}, \quad (2)$$

where $A_\Lambda = |A_\Lambda|e^{i\phi_\Lambda}$ is an amplitude with phase angle ϕ_Λ . Due to limited statistics, the mass and width of the ω meson are fixed to their world-average values [20], while the other parameters are left free during the fit. The obtained fit reveals that the observed $\rho - \omega$ interference pattern is very close to that of the cross-section measurements for the $e^+e^- \rightarrow \pi^+\pi^-$ process in the ρ/ω mass region [32–34], exhibiting a relatively narrow ρ peak. However, it differs from the measurements of the di-lepton spectra [36–38]. The fit underestimates the Λ value of $3.3 \pm 0.7 \text{ GeV}/c^2$, which is expected to be above the combined mass threshold of $m_{J/\psi\pi^0}$, due to limited statistics in the high $m_{e^+e^-}$ region. The fitted TFF function of Eq. 2 with $\Lambda = 3.686 \text{ GeV}/c^2$ is used to generate the signal MC events, while including both resonant and non-resonant contributions of $J/\psi \rightarrow e^+e^-\pi^0$, as mentioned above.

According to Eq. 1, the systematic uncertainty associated with the branching fraction and TFF measurements include those from N_{sig} , the number of J/ψ events, reconstruction efficiencies, and secondary branching fractions, details of which are described in Ref. [49]. The systematic uncertainty is dominated by the signal model (0.6%), non-peaking background PDF (2.2%), tracking efficiency (2.4%), PID (1.2%), photon reconstruction efficiency (0.4%), and E/p_{e^\pm} (2.4%). Total systematic uncertainties for the branching fraction and TFF measurements are determined to be 4.7% and 6.6%, respectively, by adding the individual ones in quadrature.

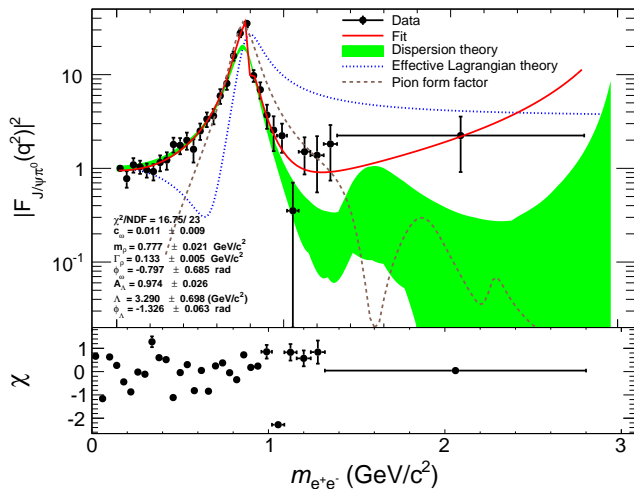


FIG. 4. (Top) Fit to the TFF versus $m_{e^+e^-}$ in data and (bottom) their pull values in each bin. The black dots with error bars are data, which include both statistical and systematic uncertainties as described in the text and Ref. [49], the blue dotted curve comes from the effective Lagrangian theory [18], the green band comes from the dispersion theory [19], brown dashed curve is the pion form factor taken from the BaBar measurement [34] and the solid red curve is the fit result, which excludes the higher-order ρ resonances.

In summary, we study the EM Dalitz decay $J/\psi \rightarrow e^+e^-\pi^0$ using a data sample of $(10087 \pm 44) \times 10^6$ J/ψ events collected by the BESIII detector. The transition form factor of this decay is studied for the first time as a function of the di-electron invariant mass. A significant peaking structure corresponding to the ρ/ω mass position is observed, which cannot be explained by the VMD model [17], effective Lagrangian [18] or dispersion theories [19]. The observed $\rho - \omega$ interference pattern closely matches that of the pionic form factor [32–34], featuring a relatively narrow ρ peak. This finding can be used to assess the accuracy of $\omega \rightarrow e^+e^-$, which is crucial for testing lepton flavour universality using a similar method of Ref. [51]. After taking into account the contribution of this resonant structure, the branching fraction of $J/\psi \rightarrow e^+e^-\pi^0$ is measured for the first time in the full $m_{e^+e^-}$ spectrum, to be $(8.06 \pm 0.31(\text{stat}) \pm 0.38(\text{syst})) \times 10^{-7}$. The measured branching fraction is two times larger than the VMD prediction [17] due to the observed resonant contribution of ρ/ω resonances.

Acknowledgement The authors thank Bastian Kubis and Zhi-Hui Guo for providing the data for their theoretical predictions. The BESIII Collaboration thanks the staff of BEPCII and the IHEP computing center for their strong support. This work is supported in part by National Key R&D Program of China under Contracts Nos. 2020YFA0406300, 2020YFA0406400, 2023YFA1606000; National Natural Science Foundation of China (NSFC) under Contracts Nos. 11635010, 11735014, 11705192,

11935015, 11935016, 11935018, 11950410506, 12025502, 12035009, 12035013, 12061131003, 12192260, 12192261, 12192262, 12192263, 12192264, 12192265, 12221005, 12225509, 12235017, 12361141819; the Chinese Academy of Sciences (CAS) Large-Scale Scientific Facility Program; the CAS Center for Excellence in Particle Physics (CCEPP); Joint Large-Scale Scientific Facility Funds of the NSFC and CAS under Contract No. U1832207; 100 Talents Program of CAS; The Institute of Nuclear and Particle Physics (INPAC) and Shanghai Key Laboratory for Particle Physics and Cosmology; German Research Foundation DFG under Contracts Nos. 455635585, FOR5327, GRK 2149; Istituto Nazionale di Fisica Nucleare, Italy; Ministry of Development of Turkey under Contract No. DPT2006K-120470; National Research Foundation of Korea under Contract No. NRF-2022R1A2C1092335; National Science and Technology fund of Mongolia; National Science Research and Innovation Fund (NSRF) via the Program Management Unit for Human Resources & Institutional Development, Research and Innovation of Thailand under Contract No. B16F640076; Polish National Science Centre under Contract No. 2019/35/O/ST2/02907; The Chilean National Agency for Research and Development ANID PIA/APOYO AFB230003 and ANID FONDECYT regular 1230987; The Swedish Research Council; U. S. Department of Energy under Contract No. DE-FG02-05ER41374

-
- [1] R. H. Dalitz, Proc. Phys. Soc. A **64**, 667 (1951).
 - [2] L. G. Landsberg, Phys. Rept. **128**, 301 (1985).
 - [3] N. M. Kroll and W. Wada, Phys. Rev. **98**, 1355 (1955).
 - [4] J. J. Sakurai, Currents and mesons, University of Chicago Press, Chicago, USA, 1969.
 - [5] V. M. Budnev and V. A. Karnakov, Pis'ma Zh. Eksp. Teor. Fiz. **29**, 439 (1979) [JETP Lett. **29**, 398 (1979)].
 - [6] G. Colangelo, M. Hoferichter, B. Kubis, M. Procura, and P. Stoffer, Phys. Lett. B **738**, 6 (2014); G. Colangelo, M. Hoferichter, M. Procura, and P. Stoffer, J. High Energy Phys. **09**, 074 (2015).
 - [7] F. Jegerlehner and A. Nyffeler, Phys. Rep. **477**, 1 (2009).
 - [8] A. Nyffeler, Phys. Rev. D **94**, 053006 (2016).
 - [9] T. Aoyama, N. Asmussen, M. Benayoun *et al.*, Phys. Rept. **887**, 1-166 (2020); G. Colangelo, M. Davier, A. X. El-Khadra *et al.*, arXiv:2203.15810[hep-ph]; B. Abi *et al.* (Muon $g - 2$ Collaboration), Phys. Rev. Lett. **126**, 141801 (2021).
 - [10] M. Hoferichter, B. Kubis, S. Leupold, F. Niecknig and S. P. Schneider, Eur. Phys. J. C **74**, 3180 (2014).
 - [11] C. Hanhart, A. Kupsc, U.-G. Meißner, F. Stollenwerk and A. Wirzba, Eur. Phys. J. C **73**, 2668 (2013).
 - [12] R. Arndt *et al.* (NA60 Collaboration), Phys. Lett. B **677**, 260 (2009).
 - [13] G. Usai *et al.* (NA60 Collaboration), Nucl. Phys. A **855**, 189 (2011).
 - [14] B. Ananthanarayan, I. Caprini and B. Kubis, Eur. Phys.

- J. C **74**, 3209 (2014).
- [15] M. Ablikim *et al.* (BESIII Collaboration), Phys. Rev. D **89**, 092008 (2014).
- [16] M. Ablikim *et al.* (BESIII Collaboration), Phys. Rev. D **99**, 012006 (2019) [Erratum: Phys.Rev.D **104**, 099901 (2021)].
- [17] J. Fu, H. B. Li, X. Qin, and M. Z. Yang, Mod. Phys. Lett. A **27**, 1250223 (2012).
- [18] Y. H. Chen, Z. H. Guo and B. S. Zhou, Phys. Rev. D **91**, 014010 (2015); L. W. Yan, Y. H. Chen, C. G. Duan and Z. H. Guo, Phys. Rev. D **107**, 034022 (2023).
- [19] B. Kubis and F. Niecknig, Phys. Rev. D **91**, 036004 (2015).
- [20] R. L. Workman *et al.* (Particle Data Group), Prog. Theor. Exp. Phys. **2022**, 083C01 (2022 and 2023).
- [21] S.L. Glashow, Phys. Rev. Lett. **7**, 469 (1961).
- [22] W. Dong, B. Yong and Li Gang, Chin. Phys. C **38**, 063101 (2014).
- [23] P. C. McNamee, M. D. Scadron and S. A. Coon, Nucl. Phys. A **249**, 483 (1975).
- [24] A. W. Thomas and K. Saito, arXiv:nucl-th/9507010; H. B. O'Connell, B. C. Pearce, A. W. Thomas and A. G. Williams, Prog. in Particle and Nucl. Phys. **39**, 201 (1997).
- [25] T. Goldman, J. Henderson J and A. Thomas, Few-Body Systems **12**, 123 (1992).
- [26] M. Shifman, A. Vainshtein and V. Zakharov, Nucl. Phys. B **147**, 519 (1979).
- [27] K. Maltman, Phys. Rev. D **53**, 2563 (1996).
- [28] R. Urech, Phys. Lett. B **355**, 308 (1995).
- [29] J. Bijnens, arXiv:hep-ph/9502393 (1995).
- [30] M. Benayoun, P. David and L. DelBuono *et al.*, Euro. Phys. Journ. C **65**, 211 (2010); Euro. Phys. Journ. C **55**, 199 (2008);
- [31] M. Benayoun and H. O'Connell, Eur. Phys. J. C **22**, 503 (2001).
- [32] F. V. Ignatov *et al.* (CMD-3 Collaboration), arXiv:2302.0883 (2023).
- [33] M. Ablikim *et al.* (BESIII Collaboration), Phys. Lett. B **753**, 629 (2016).
- [34] J. P. Lees *et al.* (BaBar Collaboration), Phys. Rev. D **86**, 032013 (2012).
- [35] A. Anastasi *et al.* (KLOE-2 Collaboration), Phys. Lett. B **767**, 485 (2017).
- [36] P. J. Biggs *et al.*, Phys. Rev. Lett. **24**, 1197 (1970).
- [37] H. Alvensleben *et al.*, Nucl. Phys. B **25**, 333 (1971).
- [38] C. Djalali, M. Paolone, D. Weygand and M. Wood, POS (Hadron 2013) 176.
- [39] M. Ablikim *et al.* (BESIII Collaboration), Nucl. Instrum. Meth. A **614**, 345 (2010).
- [40] S. Agostinelli *et al.* (GEANT4 Collaboration), Nucl. Instrum. Methods Phys. Res., Sect. A **506**, 250 (2003).
- [41] D. J. Lange, Nucl. Instrum. Methods Phys. Res., Sect. A **462**, 152 (2001); R. G. Ping, Chin. Phys. C **32**, 599 (2008).
- [42] J. C. Chen, G. Huang, X. Qi, D. Zhang, and Y. Zhu, Phys. Rev. D **62**, 034003 (2000).
- [43] L. M. Gu, H. B. Li, X. X. Ma and M. Z. Yang, Phys. Rev. D **100**, 016018 (2019).
- [44] Z. R. Xu and K. L. He, Chin. Phys. C **36**, 742 (2012).
- [45] J. M. Bian *et al.*, Int. J. Mod. Phys. A **24**, 267 (2009).
- [46] M. Ablikim *et al.* (BESIII Collaboration), Phys. Lett. B **783**, 452 (2018).
- [47] H. Czyz, S. Ivashyn, A. Korchin and O. Shekhovtsova, Phys. Rev. D **85**, 094010 (2012).
- [48] M. Ablikim *et al.* (BESIII Collaboration), Chin. Phys. C **46**, 074001 (2022).
- [49] See Supplemental Material at [URL to be inserted by the publisher] for details on the γ conversion backgrounds, non-resonant contributions, systematic uncertainties, and a table of the TFF determined in this work.
- [50] G. J. Gounaris and J. J. Sakurai, Phys. Rev. Lett. **21**, 244 (1968).
- [51] R. Aaij *et al.* (LHCb collaboration), arXiv:2402.01336 (2024).

Study of the electromagnetic Dalitz decay of $J/\psi \rightarrow e^+e^-\pi^0$: Supplemental material

I. AN ILLUSTRATION OF SIGNAL VERSUS GAMMA CONVERSION BACKGROUND EVENTS

To suppress background from $J/\psi \rightarrow \gamma\pi^0$, a γ conversion finder algorithm [1] is used. A variable $\delta_{xy} = \sqrt{R_x^2 + R_y^2}$, which is the distance from the vertex point of the e^+e^- pair to the origin in the $x-y$ plane, is used to separate the signal from the gamma conversion events. Here R_x and R_y are the coordinates of the reconstructed vertex point along the x and y directions, respectively. A distribution of R_y versus R_x from the MC simulation is shown in Fig. 1 (a), where the collected events in the center of the circle are signal events from $J/\psi \rightarrow e^+e^-\pi^0$, and the region between the inner and outer hollow circles occurred in the positions of the beam pipe and inner wall of the MDC, respectively, are background from $J/\psi \rightarrow \gamma\pi^0$. A comparison of the δ_{xy} distribution from data with the signal and background events from MC simulation is shown in Fig. 1 (b).

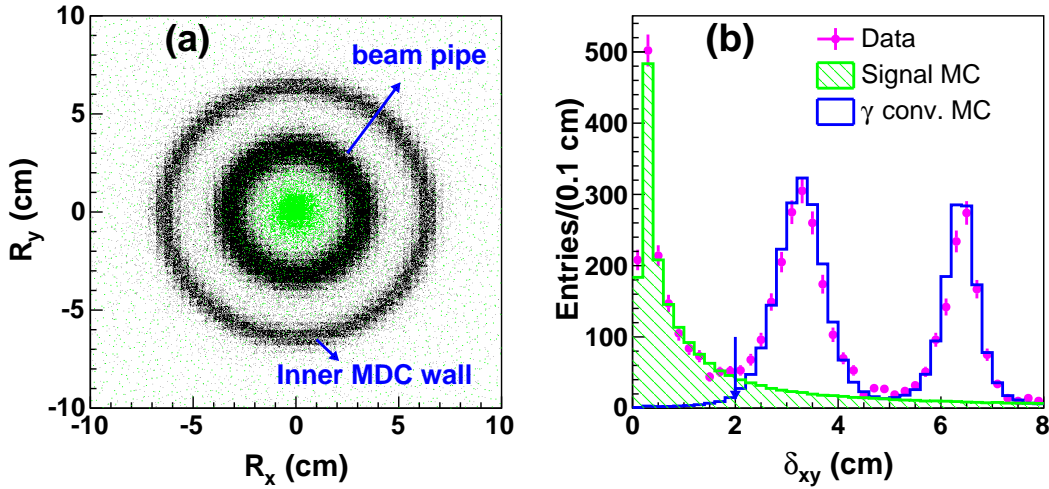


FIG. 1. (a) Distribution of R_y versus R_x for the simulated Monte Carlo (MC) events of the γ conversion process of $J/\psi \rightarrow \gamma\pi^0$ (black dot points) and signal MC events of $J/\psi \rightarrow e^+e^-\pi^0$ (green dot points), and (b) the δ_{xy} distribution of data (pink dot points with error bars), signal MC simulation (green histogram), γ conversion MC simulated events (blue histogram). The δ_{xy} requirement is shown by a solid blue arrow.

II. NON-RESONANT CONTRIBUTION OF THE $J/\psi \rightarrow e^+e^-\pi^0$

To calculate the non-resonant contribution of $J/\psi \rightarrow e^+e^-\pi^0$, the signal yield is extracted by performing a fit to the di-photon invariant mass ($m_{\gamma\gamma}$) distribution for di-electron invariant mass ($m_{e^+e^-}$) less than $0.3 \text{ GeV}/c^2$. The fit yields 992 ± 36 events, which includes both the signal and peaking background contribution from $J/\psi \rightarrow \gamma\pi^0$, $J/\psi \rightarrow \gamma\pi^0\pi^0$ and two-photon process of $e^+e^- \rightarrow e^+e^-\pi^0$, as seen in Fig. 2. Total peaking background in this mass region is predicted to be 84.9 ± 23.2 events. After subtracting the peaking background, the net signal yield (N_{sig}) is determined to be 907.1 ± 42.8 events. The efficiency of the non-resonant contribution of $J/\psi \rightarrow e^+e^-\pi^0$ is calculated to be 20.1% with a signal MC generated with a pole mass of $3.686 \text{ GeV}/c^2$ without including the resonant contribution of $J/\psi \rightarrow \rho/\omega\pi^0$. The branching fraction of $J/\psi \rightarrow e^+e^-\pi^0$ for $m_{e^+e^-} < 0.3 \text{ GeV}/c^2$ is calculated to be $(4.41 \pm 0.18 \pm 0.21) \times 10^{-7}$, where the first and second uncertainties are statistical and systematic, respectively.

III. SYSTEMATIC UNCERTAINTIES RELATED TO THE BRANCHING FRACTION AND TRANSITION FORM FACTOR MEASUREMENTS

The systematic uncertainty associated with the signal modelling is evaluated to be 0.6% by replacing their shapes from the simulated MC samples by the sum of the two crystal ball (CB) functions [2]. The systematic uncertainty

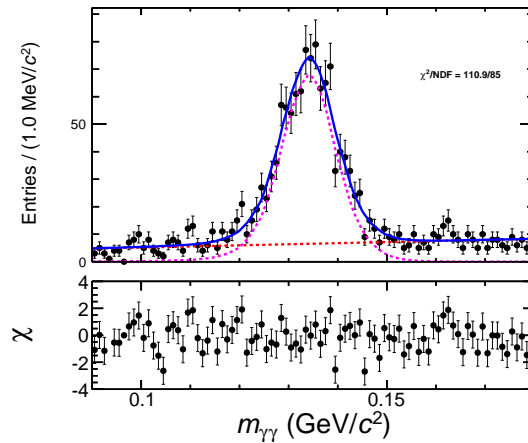


FIG. 2. Fit to the $m_{\gamma\gamma}$ distribution of J/ψ data for $m_{e^+e^-} < 0.3 \text{ GeV}/c^2$ (top) together with the distribution of normalized fit residuals (bottom). The black dots with error bars represent the data, the pink dashed curve the signal PDF and the red dashed curve the non-peaking PDF. The solid blue curve is the total fit result.

of the non-peaking background PDF is evaluated to be 2.2% by replacing the corresponding function with a 2nd order Chebyshev polynomial function in the fit. The reliability of the fit is validated by producing a large number of pseudo-experiments containing the same statistics as that of the data. The same fit procedure is performed in each pseudo-experiment, and we consider the relative average difference between the input and output signal yields, which is 0.3%, as one of the systematic uncertainties.

A control sample of the radiative Bhabha process $e^+e^- \rightarrow \gamma e^+e^-$ is used to explore the efficiencies of tracking and particle identification (PID) for e^\pm in the different 2-dimensional bins of momentum versus polar angle. The resulting average differences in efficiency between data and MC are weighted according to the momentum and polar angle of the signal MC, and determined to be 1.2% for tracking and 0.6% for the PID considered for each charged track as systematic uncertainties. The photon detection efficiency is studied with a control sample of radiative muon-pair events at J/ψ resonance in which the initial-state-radiation (ISR) photon is predicted using the four-momenta of two charged tracks. The relative difference in efficiency between data and MC is observed to be up to the level of 0.2%, and considered to be as systematic uncertainty [3]. The total systematic uncertainties associated with the tracking, PID and photon reconstruction efficiency are evaluated to be 2.4%, 1.2% and 0.4%, respectively.

The systematic uncertainty for the $\delta_{xy} < 2 \text{ cm}$ requirement is studied with a control sample of $J/\psi \rightarrow \pi^+\pi^-\pi^0$, $\pi^0 \rightarrow \gamma e^+e^-$. The signal MC sample for $\pi^0 \rightarrow \gamma e^+e^-$ is generated with a simple pole approximation transition form factor (TFF), $F(q^2) = 1 + a_\pi q^2/m_{\pi^0}^2$, where m_{π^0} is the nominal π^0 mass and $a_\pi = 0.031 \pm 0.004$ is a slope parameter [4]. In order to separate the signal from the background contribution of $\pi^0 \rightarrow \gamma\gamma$ in this control sample, the ML fit to the $m_{\gamma\gamma}$ distribution is performed before and after the selection of $\delta_{xy} < 2 \text{ cm}$ requirement. The corresponding relative difference in efficiencies between data and MC is observed to be 0.12%, and taken as the systematic uncertainty. The systematic uncertainty associated with the selection criteria of E/p_{e^\pm} is evaluated to be 1.2% for each charged track with a total of 2.4% using the same control sample of $J/\psi \rightarrow \pi^+\pi^-\pi^0$, $\pi^0 \rightarrow \gamma e^+e^-$. A control sample $J/\psi \rightarrow \pi^+\pi^-\pi^0$, $\pi^0 \rightarrow \gamma\gamma$ is utilized to study the systematic uncertainty associated with the 4C kinematic fit, which is calculated to be 0.4%. The background contribution of $\pi^0 \rightarrow \gamma e^+e^-$ in this control sample is eliminated by requiring $|\cos\theta_{\text{heli}}| < 0.9$, where θ_{heli} is the angle between the direction of one of the photons and J/ψ direction in the π^0 rest frame. The relative difference in efficiency between data and MC, found to be 0.3%, is considered as systematic uncertainty.

We vary the requirements of e^\pm momentum, $\cos\theta(e^\pm)$ and the lowest energy of photon used for $\pi^0 \rightarrow \gamma\gamma$ reconstruction within one standard deviation of the statistical uncertainties to study the systematic uncertainty of the requirements of these variables. One of the largest values of the relative difference between the signal yields of $J/\psi \rightarrow e^+e^-\pi^0$ is 0.4%, considered as the systematic uncertainty. In the branching fraction measurement of $J/\psi \rightarrow e^+e^-\pi^0$ in the full $m_{e^+e^-}$ range, the simulated MC events, used for the determination of the detection efficiency, are generated with the fit function of TFF measured in this analysis with the Λ value of $3.686 \text{ GeV}/c^2$. Two alternative signal MC samples with the simple pole mass Λ values of $3.1 \text{ GeV}/c^2$ and $4.0 \text{ GeV}/c^2$ are generated. One alternative signal MC sample is also generated with the $\rho - \omega$ resonance parameters of dipion channel [5]. One of the largest relative difference in efficiencies is 0.9%, which is considered as systematic uncertainty. The systematic uncertainty of the J/ψ counting is evaluated to be 0.44% using the inclusive hadronic events of the J/ψ decays.

IV. DI-ELECTRON INVARIANT MASS DEPENDENT TRANSITION FORM FACTOR

TABLE I. Background subtracted N_{sig}^i , the measured and quantum electrodynamics (QED) predicted $\mathcal{B}(J/\psi \rightarrow e^+e^-\pi^i)$ differential branching fraction (BF) and the transition form factor (TFF) $|F(q^2)|^2$, for all 44 bins. The first uncertainty is statistical and the second is systematic. Obtained signal yield also includes the total uncertainty of the peaking backgrounds. The QED prediction includes the uncertainty on the branching fraction measurement of $J/\psi \rightarrow e^+e^-\pi^0$.

Mass (GeV/ c^2)	N_{sig}	BF (10^{-8})	QED BF (10^{-8})	TFF
0.02 ± 0.02	628.99 ± 28.88 ± 39.15	23.50 ± 1.10 ± 1.50	19.40 ± 0.93	1.21 ± 0.06 ± 0.08
0.06 ± 0.02	56.10 ± 10.30 ± 4.33	3.58 ± 0.66 ± 0.28	3.82 ± 0.18	0.94 ± 0.17 ± 0.07
0.10 ± 0.02	50.20 ± 8.25 ± 3.19	2.94 ± 0.48 ± 0.19	2.23 ± 0.11	1.32 ± 0.22 ± 0.08
0.14 ± 0.02	67.50 ± 9.89 ± 4.40	1.98 ± 0.29 ± 0.13	1.58 ± 0.08	1.26 ± 0.18 ± 0.08
0.18 ± 0.02	53.80 ± 8.53 ± 3.40	1.41 ± 0.22 ± 0.09	1.22 ± 0.06	1.16 ± 0.18 ± 0.07
0.22 ± 0.02	41.60 ± 7.74 ± 2.79	1.11 ± 0.21 ± 0.07	0.99 ± 0.05	1.12 ± 0.21 ± 0.08
0.26 ± 0.02	43.30 ± 7.84 ± 2.88	1.16 ± 0.21 ± 0.08	0.83 ± 0.04	1.39 ± 0.25 ± 0.09
0.30 ± 0.02	37.80 ± 7.55 ± 2.59	1.06 ± 0.21 ± 0.07	0.72 ± 0.03	1.48 ± 0.30 ± 0.10
0.34 ± 0.02	48.90 ± 8.29 ± 3.06	1.36 ± 0.23 ± 0.09	0.63 ± 0.03	2.17 ± 0.37 ± 0.14
0.38 ± 0.02	43.30 ± 7.98 ± 2.94	1.18 ± 0.22 ± 0.08	0.56 ± 0.03	2.13 ± 0.32 ± 0.14
0.42 ± 0.02	33.10 ± 6.54 ± 2.10	1.20 ± 0.24 ± 0.08	0.50 ± 0.02	2.41 ± 0.48 ± 0.15
0.46 ± 0.02	23.20 ± 6.18 ± 1.79	0.87 ± 0.23 ± 0.07	0.45 ± 0.02	1.93 ± 0.52 ± 0.15
0.50 ± 0.02	33.90 ± 6.40 ± 2.14	1.24 ± 0.23 ± 0.08	0.41 ± 0.02	3.03 ± 0.57 ± 0.19
0.54 ± 0.02	41.00 ± 6.85 ± 2.55	1.51 ± 0.25 ± 0.09	0.37 ± 0.02	4.05 ± 0.68 ± 0.25
0.58 ± 0.02	39.10 ± 6.86 ± 2.44	1.50 ± 0.26 ± 0.09	0.34 ± 0.02	4.39 ± 0.77 ± 0.27
0.62 ± 0.02	58.50 ± 8.81 ± 5.66	2.26 ± 0.34 ± 0.22	0.31 ± 0.02	7.17 ± 1.08 ± 0.70
0.66 ± 0.02	70.20 ± 9.28 ± 4.37	2.83 ± 0.37 ± 0.18	0.29 ± 0.01	9.75 ± 1.29 ± 0.61
0.70 ± 0.02	138.00 ± 13.00 ± 8.64	5.17 ± 0.49 ± 0.32	0.27 ± 0.01	19.20 ± 1.81 ± 1.20
0.74 ± 0.02	214.00 ± 15.10 ± 13.30	8.36 ± 0.59 ± 0.52	0.25 ± 0.01	33.50 ± 2.37 ± 2.08
0.78 ± 0.02	261.00 ± 17.00 ± 16.20	9.88 ± 0.65 ± 0.61	0.23 ± 0.01	42.60 ± 2.78 ± 2.64
0.82 ± 0.02	68.40 ± 8.88 ± 4.33	2.55 ± 0.33 ± 0.16	0.22 ± 0.01	11.80 ± 1.53 ± 0.75
0.86 ± 0.02	40.70 ± 7.42 ± 3.08	1.68 ± 0.31 ± 0.13	0.20 ± 0.01	8.36 ± 1.52 ± 0.63
0.90 ± 0.02	22.10 ± 6.13 ± 1.69	0.84 ± 0.23 ± 0.06	0.19 ± 0.01	4.49 ± 1.24 ± 0.34
0.94 ± 0.02	14.40 ± 5.45 ± 2.01	0.54 ± 0.21 ± 0.08	0.18 ± 0.01	3.10 ± 1.17 ± 0.43
0.99 ± 0.03	17.00 ± 5.12 ± 2.83	0.65 ± 0.20 ± 0.11	0.24 ± 0.01	2.70 ± 0.81 ± 0.45
1.050 ± 0.035	2.58 ± 1.58 ± 2.02	0.11 ± 0.07 ± 0.08	0.25 ± 0.01	0.43 ± 0.26 ± 0.33
1.120 ± 0.035	10.20 ± 4.27 ± 0.84	0.41 ± 0.17 ± 0.03	0.22 ± 0.01	1.82 ± 0.76 ± 0.15
1.20 ± 0.04	9.69 ± 5.67 ± 1.20	0.38 ± 0.22 ± 0.05	0.23 ± 0.01	1.67 ± 0.98 ± 0.21
1.28 ± 0.04	9.82 ± 5.69 ± 1.23	0.43 ± 0.25 ± 0.05	0.20 ± 0.01	2.20 ± 1.28 ± 0.28
2.06 ± 0.74	59.70 ± 35.10 ± 3.85	2.63 ± 1.50 ± 0.17	0.97 ± 0.05	2.71 ± 1.60 ± 0.18
Total BF		84.30 ± 2.57 ± 1.81		

-
- [1] Z. R. Xu and K. L. He, Chin. Phys. C **36**, 742 (2012).
[2] J. E. Gaiser, Ph. D. Thesis, SLAC-R-255 (1982) (unpublished); M. J. Oreglia, Ph. D. Thesis, SLAC-R-236 (1980) (unpublished); T. Skwarnicki, Ph.D. Thesis, DESY-F-31-86-02 (1986) (unpublished).
[3] M. Ablikim *et al.* (BESIII Collaboration), Phys. Rev. D **105**, 012008 (2022).
[4] R. L. Workman *et al.* (Particle Data Group), Prog. Theor. Exp. Phys. **2022**, 083C01 (2022 and 2023).
[5] M. Ablikim *et al.* (BESIII Collaboration), Phys. Lett. B **753**, 629 (2016).